Cardiovasc Eng
DOI 10.1007/s10558-008-9061-0

ORIGINAL PAPER

Estimation of *Nonlinear* Mechanical Properties of Vascular Tissues via Elastography

Reza Karimi · Ting Zhu · Brett E. Bouma · Mohammad R. Kaazempur Mofrad

Abstract A new method is proposed for estimation of *nonlinear* elastic properties of soft tissues. The proposed approach involves a combination of nonlinear finite element methods with a genetic algorithm for estimating tissue stiffness profile. A multipoint scheme is introduced that satisfies the uniqueness condition, improves the estimation performance, and reduces the sensitivity to image noise. The utility of the proposed techniques is demonstrated using optical coherence tomography (OCT) images. The approach is, however, applicable to other imaging systems and modalities, as well, provided a reliable image registration scheme. The proposed algorithm is applied to realistic (2D) and idealized (3D) arterial plaque models, and proves promising for the estimation of intra-plaque distribution of nonlinear material properties.

Keywords Soft tissue mechanics · Nonlinear material properties · Atherosclerosis · Elastography · Genetic algorithm · Optical coherence tomography

R. Karimi · T. Zhu
Department of Mechanical Engineering, Massachusetts Institute of Technology, Cambridge, MA 02139, USA

R. Karimi · M. R. Kaazempur Mofrad (✉)
Department of Bioengineering, University of California, 208A Stanley Hall #1762, Berkeley, CA 94720, USA
e-mail: mofrad@berkeley.edu

B. E. Bouma
Wellman Center for Photomedicine, Massachusetts General Hospital, Harvard Medical School, Boston, MA, USA 02114

Introduction

Cardiovascular disease is a leading cause of morbidity and mortality, primarily through atherosclerotic plaque formation and rupture often followed by myocardial infarction or acute cerebral stroke (Thom et al. 2006). Elevated levels of (cyclic) strain/stress are believed to be likely indicators of unstable plaques (Kaazempur-Mofrad et al. 2003; Lee et al. 1996; Loree et al. 1992; Richardson et al. 1989). This has motivated recent efforts to construct quantitative images of strain, named elastograms, and elasticity modulus distribution for assessment of the stability or vulnerability of the atherosclerotic plaques. Arterial elastograms and modulus distribution patterns will provide further insight into plaque morphology, composition, biomechanics and rupture risk (Fig. 1) (Baldewsing et al. 2005; Lee et al. 1993; Schaar et al. 2003, 2004).

Stress is a local quantity describing force carried by an object normalized by the area on which the force acts. Force application introduces deformation on the object. Deformation is typically described by strain, which has the units of length change over length. Strain can vary with spatial coordinates and the elastogram is the graph that depicts the strain variations over a certain area or volume. Elastography deals with elastograms and hence begins with image registration, i.e. identifying how each image point corresponding to a single material point of tissue is moving within different frames. The gradient of the displacement field, computed in the registration step, generates the strain (tensor) field or elastogram (Ophir et al. 1991).

Elastography was originally developed as a quantitative palpation technique to diagnose breast cancer with ultrasound (Ophir et al. 1991). Arterial elastography is more challenging than breast tissue elastography due mainly to the smaller length scales involved, time varying blood flow

Published online: 02 December 2008

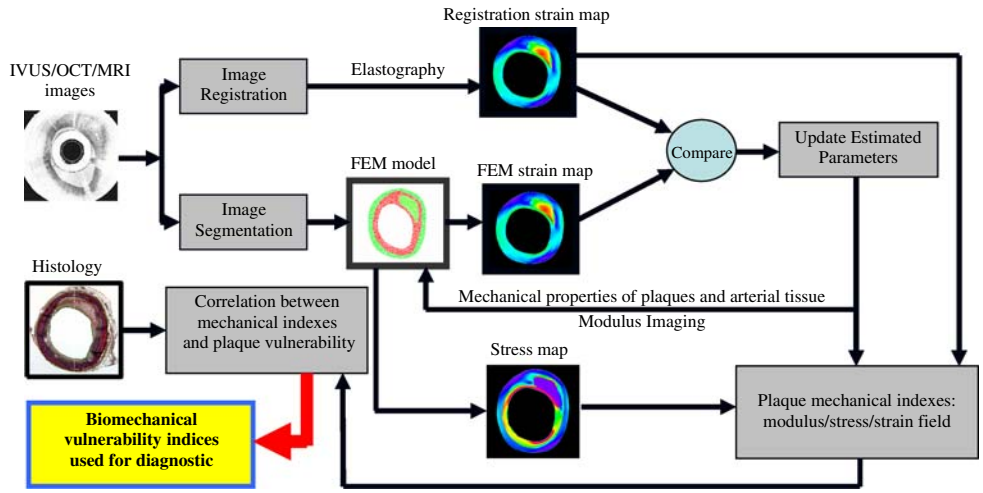

Fig. 1 Overall flow chart of the elastography and parameter estimation procedures for arterial plaque characterization. Frames of images, as obtained with IVUS/OCT/MRI modalities, are registered to find the strain map. The images are segmented to build a lumped mechanical model. Then an iterative scheme is used to match the strain computed by image registration and the mechanical model. Finally, when the process converges, a reliable strain/stress/modulus map is achieved. This map can be validated with histological markers of plaques (including their vulnerability level) and can then be used to build biomechanical indices for plaques vulnerability and evolutions

and presence of several plaques with different sizes, geometries, and compositions. Breast elastography typically deals with a large single inclusion that is usually less than ten times stiffer than the normal breast tissue (Ophir et al. 1997). On the contrary, modulus of lipid pools in atherosclerotic plaques can alone span four orders of magnitudes (Duck 1990). Moreover, a time varying pressure is exerted on the arterial plaques, whereas static compression forces are often used in breast elastography.

Extensive efforts have been devoted to developing elastography. Intravascular ultrasound (IVUS) has been successfully used to estimate the arterial radial strain, despite its limited resolution (Baldewsing et al. 2005; Schaar et al. 2003, 2004). However, a drawback in IVUS elastography is that the catheter must be located at the center of artery and hence IVUS is only capable of registering axial displacement. Correlation-based OCT elastography (Chan et al. 2004), does not have this limitation. OCT elastography based on Doppler or phase information is however also limited to estimating radial motion (Wang et al. 2007). The MRI (visco) elastography has been also developed extensively (Sinkus et al. 2005), but not applied to arterial wall, due mainly to its lower resolution.

Stress and strain are related through material constitutive relations. The simplest form of such relations is the isotropic linear elastic model, which has only one unknown for incompressible materials. That unknown is called the (elastic) modulus. Traditional elastography protocols typically assume a 'constant stress field', implying that elastogram is equivalent to the modulus image (for incompressible tissue with isotropic linear elastic behavior). However, arteries are typically characterized by asymmetric geometries, which together with the presence of plaques with varying compositions lead to a nonhomogeneous stress field in arterial wall. This prevents a direct match between strain levels and stress or modulus images. In such cases, the displacement field can still be used to find the elastic modulus field but requires a more elaborate solution strategy. This type of problem is called the inverse elasticity problems (Kallel and Bertrand 1996), in contrast to a simpler case of direct (or forward) elasticity problem wherein the displacement field is computed for a known modulus field.

Conventionally 'gradient-based techniques' are used to solve the inverse elasticity problem, allowing to resolve elastic properties on a fine mesh (Doyley et al. 2000; Kallel and Bertrand 1996; Khalil et al. 2005; Oberai et al. 2004). Since elastic properties in arterial plaque can span four orders of magnitude (Duck 1990), gradient-based parameter estimation techniques face several challenges, e.g. lack of accurate estimation of the relatively softer regions of the plaque, necessity of finding a 'good' initial guess and adopting higher error levels due to regularization.

As an alternative to gradient-based techniques or at least as a means for providing a reasonably good initial guess for gradient-based methods, we previously introduced a new approach using genetic algorithm (GA) (Khalil et al. 2006). In this approach, the intraplaque boundaries are used to divide different regions of plaque into lumped areas with the same elastic properties. The GA-based approach is viable and effective in dealing with parameters of different

orders. Furthermore, the GA-based approach can generate a coarse-grained map of elasticity distribution serving as a robust and preconditioned initial guess for fine mesh computations. This approach enables us to find the global minima that cannot be captured by gradient-based methods. Moreover, the elastic modulus computed by GA can also serve as a lumped or effective elasticity map that can be easily utilized for correlation with medical indexes of interest (Khalil et al. 2006; Schaar et al. 2004).

The GA-based approach is an efficient technique that provides accurate measurement of soft tissue linear isotropic elastic modulus (Khalil et al. 2006). Encouraged by the initial success of our GA-based approach for estimation of linear mechanical properties of atherosclerotic plaques, we set out to extend this approach to account for *nonlinear* constitutive relations, representative of vascular tissues. It is well known that arterial tissues exhibit a nonlinear behavior and experience high cyclic strain levels in each single cycle of heart beat, namely as large as 10% for carotid bifurcation (Kaazempur-Mofrad et al. 2003; Loree et al. 1992) or 20% at thoracic aorta (Draney et al. 2002). Consequently, to limit the analysis to the linear regime, IVUS-based elastography relies on radial linear stain, using two closely correlated frames (Schaar et al. 2003). However, we are interested to ascertain the tissue's nonlinear behavior to resolve the more realistic loading regimes that plaques experience. Furthermore, conventional OCT might have an appreciably lower framing rate, namely 10–15 frames per second (fps) as opposed to 60 fps for IVUS, and consequently it might be more likely to deal with nonlinear and large scale deformations of arteries. The lower framing rate might be resolved by using newer frequency domain generations of OCT that allow for higher framing rates of $>$30 fps (Yun et al. 2003). Nevertheless our technique would still be viable for two reasons. First, there is no alternative in vivo measurement technique for estimation of nonlinear parameters. Moreover, if the frames correspond to largely different pressure levels, the strain will be increasingly more accurate due to higher signal to noise ratio of the registration, provided that the strain induced speckle decorrelation is not overly excessive.

The objective of this paper is, therefore, to extend our elastography efforts in mechanical characterization of arteries (Chan et al. 2004; Khalil et al. 2005, 2006) to *nonlinear* regime. Here we will employ sharp boundaries (for example as provided by high contrast images of OCT) for lumped parameter estimation. Preliminary results are presented using realistic 2D and idealized 3D arterial plaque models to evaluate the proposed GA-based nonlinear elasticity estimation technique.

The present work is based on utilizing intravascular optical coherence tomography (OCT) as an imaging modality that offers a relatively high contrast and resolution as compared to IVUS. The proposed techniques for estimation of nonlinear material properties are, however, generic with respect to imaging modality and can be implemented with other imaging modalities. OCT does, however, allow for direct extraction of morphological boundaries of common arterial tissue types (Yabushita et al. 2002). This additional information was utilized to solve the inverse elasticity problem and to accurately evaluate the isotropic linear elastic properties of arterial tissues in our previous work (Khalil et al. 2005, 2006).

The remainder of this paper is organized as follows. Section "Backgrounds and methods" covers including OCT imaging, parameter estimation based on genetic algorithm and finite element modeling (FEM) of arterial tissues. Section "Results" presents results of nonlinear parameter estimation using genetic algorithms and random exhaustive search. Finally, section "Discussion" discuses remaining challenges, error sources and future improvements for the present approach.

Backgrounds and Methods

OCT Imaging and Elastography of Arteries

Various imaging modalities like IVUS and magnetic resonance imaging (MRI) have been developed for characterization of atherosclerotic plaques (Nighoghossian et al. 2005). Vulnerable plaques are typically characterized by a thin shoulder (0.06–0.2 mm), which is well beyond the resolution of conventional imaging techniques. Consequently we aim to utilize catheter-based OCT which has up to 0.01 mm resolution, and thereby is an ideal and unique modality for accurate identification of vulnerable plaques (Fercher et al. 2003).

In OCT a beam of near infrared light is split into two, one sent into the sample and one used as the reference beam. Then optical interferometry is used to build an image upon the back-reflections of tissue. Axial direction is scanned by varying the optical path-length of the reference arm and the lateral direction is covered by rotating the sample beam. Compared to IVUS, OCT offers superior resolution and higher tissue contrast, but has higher noise, lower penetration depth and is still an invasive technique.

Catheter-based OCT generates high-resolution images and is capable of identifying arterial tissue types directly (Yabushita et al. 2002). A drawback of OCT is its low penetration depth (2–3 mm), but this depth is still enough for the study of vulnerable plaques, which are usually located near lumen surface (Tearney et al. 2006). Meanwhile, OCT is characterized by a relatively high speckle noise and low imaging rate, hence its registration requires careful attention. Although OCT is the optical analog of

ultrasound B-mode, the conventional IVUS-based elastography techniques have not been successfully applicable to OCT (Rogowska et al. 2004; Schmitt 1998). Newer robust registration methods are therefore needed which are specialized for OCT (Chan et al. 2004; Karimi et al. 2006). In this work we utilize OCT images for building realistic arterial models and use them to simulate artificial elastography data. Future work will directly rely on registered elastography data.

Two-dimensional (2D) OCT sections of excised coronary arteries were obtained according to our previously described protocol (Chau et al. 2004). Framing rate was 4 fps and the pullback rate was equal to 0.5 mm/s. The axial and transverse resolutions were 10 and 25 μm, respectively, corresponding to 500 angular pixels × 250 radial pixels. OCT segmentation was performed by expert OCT readers using previously published criteria for tissue classification (Yabushita et al. 2002).

Here OCT images were used for simulation only; hence the framing rate and other related details do not matter. Yet, a brief description of eventual intravascular OCT elastography setup is provided for completeness. In practice we plan to use high speed OCT like our newly published setup with at least 108 fps (Yun et al. 2006). The pullback rate is set such that each section is imaged for at least one full cycle of heartbeat. The images can be low sampled via median filtering in the time domain to reduce the image noise and yet we can easily achieve 24 frames per heart cycle. Low diameter catheter is used and saline is injected for OCT imaging, relying on blood pressure as driving force (i.e. not using an occlusion balloon). We have already developed techniques for 3D registration and will use them for estimation of 3D displacement vectors at nodes corresponding to our finite element model (FEM). The strain map obtained with elastography then can be compared with strain calculated from FEM model to update and improve our estimate of mechanical properties.

Finite Element Modeling

Finite element models, both in 2D and 3D, were employed to test the viability of the proposed estimation algorithm. Digital images were processed, imported into a commercially available FEM package ADINA (Watertown, MA), and used to construct finite element models (Fig. 2a). 3D models can be made by combining multiple cross sections obtained via pullback. We have published an example of a 3D reconstructed coronary artery (Yun et al. 2006). Recently the dimensions of coronary stents have been measured with OCT pullback in vivo and have been compared with direct and IVUS measurements. It has been shown that the geometries obtained with this method are reproducible and accurate and hence we expect that we can build reasonably accurate 3D models with OCT pullback (Kawase et al. 2005; Yun et al. 2006). However, the tissue segmentation in 3D cases is rather tedious and for simplicity here we rely on a simulated 3D plaque model, given that our focus in this paper is on the parameter estimation techniques. Our 3D model consists of a cylindrical arterial segment with a crescent-shaped fibrous plaque and a spherical lipid pool (Fig. 2b).

In both 2D and 3D cases, pressure is prescribed on the inner and outer layers of arteries. The lumen pressure is applied gradually, increasing from 0 to 16 kPa (120 mmHg) in 24 time steps. The initial 80 mmHg pressure serves as preloading and 80–120 mmHg pressure range represents the physiological oscillation. Strain fields calculated at each loading step are utilized as fictitious elastography data in our current characterization study. In practice, they will be obtained experimentally by registering consecutive imaging frames. No axial movement is allowed for end segments to mimic plane strain assumption and one node in lower segment is totally fixed to avoid rigid body motion. Specifically, 9-node 2D plane strain elements and pyramid 4-node 3D elements, both with mixed (u,p) interpolation, are utilized with a sufficient mesh density determined based on grid convergence studies.

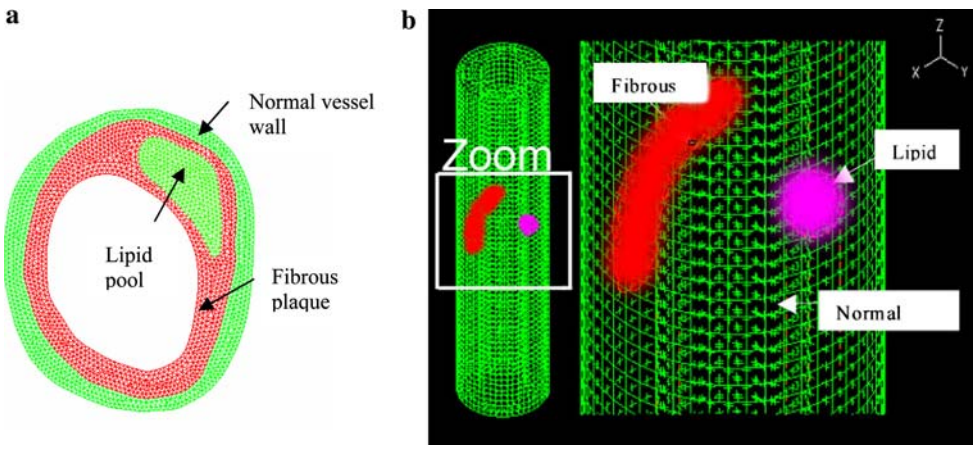

Fig. 2 Finite element models. **a** 2D geometry of OCT-derived image of segmented atherosclerotic vessel. **b** Finite element mesh of a 3D idealized arterial segment and solid bodies of a fibrous plaque and a lipid pool

Table 1 True values of Mooney-Rivlin parameters and search fields for RES/GA used for different regions of the arterial plaque

Mooney-Rivlin parameters	True values		Search field for RES		Search field for GA	
	D_1 [Pa]	D_2	D_1 [Pa]	D_2	D_1 [Pa]	D_2
Arterial wall	2644.7	8.4	2000–4000	7–10	1000–10000	1–10
Fibrous plaque	5105.3	13.0	4000–6000	10–14	1000–10000	10–100
Lipid	50.0	0.5	20–60	0.3–0.6	10–100	0.1–1

The Mooney-Rivlin model (Bathe 1996; Rivlin 1948) is used to estimate the mechanical behavior of the corresponding regions in the FEM model, namely normal vessel wall, fibrous plaque, and lipid pool. This model is defined by the strain energy density function:

$$W = D_1\left(e^{D_2(I_1-3)} - 1\right) \tag{1}$$

where D_1 and D_2 are material constants, and I_1 is the first invariant of the Cauchy-Green deformation tensor. The product D_1D_2 is proportional to the elastic modulus of the material and D_2 is related to strain-stiffening behavior. The values for D_1 and D_2 were taken from previous literature (see Table 1; Huang et al. 2001).

Parameter Estimation

Fitness Function

An estimation method is composed of defining a fitness function and choosing an iteration scheme. The iteration (or update) scheme is implemented to update the solution guess for the next step, based on the best solutions of the current step. Usually a certain number of possible solutions must be examined via a fitness function. Here, an effective strain, computed at the center of each finite element, is used for fitness evaluation:

$$\text{Effective Strain} = \sqrt{e_{xx}^2 + e_{yy}^2 + \frac{1}{2}e_{xy}^2}, \tag{2}$$

x,y: directions in axial sections

The error in effective strain is divided by the number of elements corresponding to a particular region and then the second (L_2) norm of this vector is interpreted as a fitness measure for that region. Total fitness is defined as the equally weighted summation of individual fitness measures. The same effective strain is used for 3D cases, because the cyclic strain in longitudinal direction is small and also difficult to measure.

Multipoint Scheme

Uniqueness is a central concern in the parameter estimation realm. Some elementary sufficient conditions for unique estimation of linear homogeneous elastic models in inverse elasticity problem are extracted (Barbone and Bamber 2002). One of those conditions is to know the displacement field in different independent loading conditions. This is not usually feasible in linear problems in practice, but it is valuable for nonlinear models where almost all load settings result in linearly independents displacements. However, the problem is far more complicated in the nonlinear models due to extra unknowns. Consequently, the knowledge of one loading point will not be at all sufficient to find a unique solution. For instance, the Mooney-Rivlin model requires a minimum of two (displacement/strain) points to uniquely capture the stress-strain curve. Moreover, the result of the estimation is sensitive to the noise and the uncertainty in the elastography data. Thus to ensure the uniqueness of the solution as well as reducing noise effect, we propose to use multiple loading points at incremental pressure loads and we refer to it as a multipoint scheme. Note that the multiple image frames are distinct from multiple data points of displacement/strain. Indeed we have an extra base image frame with respect to which the displacement field is computed. For example, if we have 10 image frames, the multipoint scheme can rely on at most 9 strain frames/points.

Here we use evenly spaced pressure increments to generate multiple points of strain data, but in practice we must rely on increments associated with fixed time interval. As a result, by fitting the stress–strain curve to a number of linearly independent points, we expect to obtain an optimized robust unique solution.

Genetic Algorithm

Another aspect of a parameter estimation technique is the way that the guess is updated. Here we use random exhaustive search (RES) and genetic algorithm (GA) (Haupt and Haupt 2004; Khalil et al. 2006). RES is mainly used for discrete problems in which no efficient solution method is known, making it necessary to test each possibility sequentially in order to determine the solution. Such exhaustive examination of all possibilities is known as ‘exhaustive search’, ‘direct search’, or the ‘brute force method’ (Fig. 3a; Haupt and Haupt 2004). A large number of guesses are generated and examined to search for the

best solution. It must be emphasized that the RES technique is highly inefficient and is used here only to evaluate feasibility of nonlinear mechanical parameter estimation and to assess the effectiveness of GA.

Genetic algorithm is expected to be a 'smarter' and more effective way of finding the best solution. In GA, a small set of initial guesses is created and by evaluating their fitness a next generation of guesses is generated. The update scheme in GA simulates biological evolution through naturally occurring genetic operations on chromosomes (Haupt and Haupt 2004). GA applies the Darwinian principle of 'survival of the fittest' on string structures to build unique searches with elements of structure and randomness (Fig. 3b). RES can be considered as a limiting case of GA, having a large population in which GA stops after the first iteration. Genetic algorithms begin with a predefined initial population of 'individuals', typically created at random from a field of possible solutions. Through pseudo-genetic operations, such as mating pool selection, crossover reproduction, and mutation, the fittest individuals in the population survive to the next generation and facilitate the proliferation of new individuals.

The settings of GA operations largely follow our previous work with linear constitutive relations (Khalil et al. 2006). However, to explore a wider range of unknowns and a great degree of randomness in the population size, our GA method must be extended to incorporate a 'mutation' operation. Mutation operation involves addition of a stream of independently generated random parameters, or 'new blood', into the population in each step. The purpose of mutation in genetic algorithm is to increase evolution rate as well as to avoid local minima by preventing individuals to become very similar to each other at early stages of evolution.

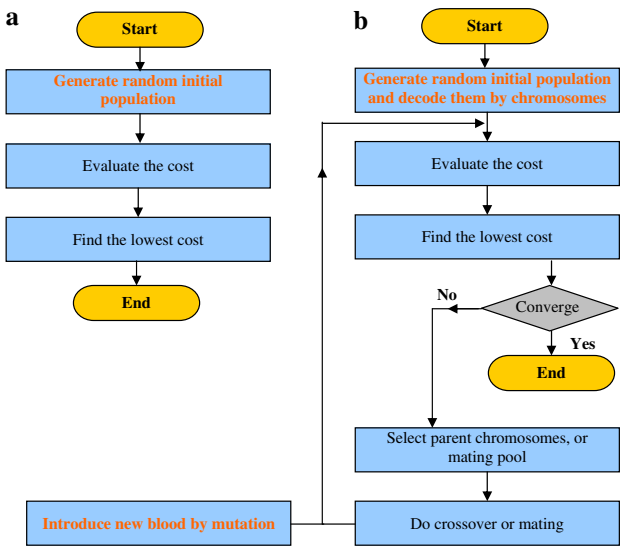

Fig. 3 **a** Flowchart of random exhaustive search. **b** Flowchart of genetic algorithm

Results

Random Exhaustive Search

To assess the utility of multipoint scheme and the feasibility of nonlinear mechanical parameter estimation, we utilized the random exhaustive search (RES) method. Since the RES solution is highly sensitive to its randomly generated initial population, we repeated the solution procedure for many (namely 8) times and used the mean and standard deviation of the solution to quantify our evaluation.

An initial population was generated randomly with 400 sets of 6 material parameters (D_1 and D_2 for arterial wall, fibrous plaque, and lipid pool) in the search field (Table 1). Different white Gaussian noise levels, namely 1%, 5%, and 10%, were added to the elastography strain data to test the sensitivity of the overall multipoint algorithm. Consequently, the robustness of the parameter estimation algorithm was tested against the noise using both single point and multipoint schemes. Furthermore, the effect of pressure inaccuracy on the parameter estimation was assessed by applying 1%, 5%, and 10% pseudo errors in pressure. As a result the computed displacement field inherited the corresponding error due to variations in the force boundary condition.

Using 2 data points, noise free data produces estimated parameters fairly accurately (see Table 2). However, a considerable error is always observed in the estimation of lipid parameters. This can be associated with the 'near-singular' behavior of lipid pool. That is, a small change in the magnitude (although large in percentage) of lipid's mechanical property yields negligible effect on the overall strain map. However, some normalizing techniques can alleviate poor lipid estimation as implemented in our previous work (Khalil et al. 2006). Nevertheless, thanks to the minimal contribution of the lipid to the overall stress field, the stress calculation in atherosclerotic vessel wall is not compromised. To evaluate the overall error in each case, we used the average error for the material parameters

Table 2 Estimation results with 2-point RES using noise-free data

Mooney-Rivlin parameters	2-frame estimated results (based on 8 runs)	
	D1 [Pa] (error) ± SD	D2 (error) ± SD
Arterial wall	2613.4 (1.2%) ± 7.1%	8.5 (1.2%) ± 5.2%
Fibrous plaque	4966.2 (2.7%) ± 2.3%	13.0 (0.3%) ± 1.0%
Lipid	43.4 (13.2%) ± 20.2%	0.5 (5.9%) ± 19.5%

excluding the lipid pool, which has a relatively large standard deviation and yet minor mechanical role. Note that since lipid elasticity modulus is approximately two orders of magnitude lower than the other constituents, it is not reasonable to directly compare its relative error with other constituents, given that its absolute error is very insignificant compared to others.

The sensitivity of the algorithm to the image (strain) noise was next evaluated using different levels of noise and different numbers of data points. The overall error decreased as the number of points used in the algorithm was increased (Fig. 4a). In presence of 1% strain noise, using 12-loading points instead of 2-loading points lowers the estimation error by approximately 6-fold, demonstrating the utility of the multipoint technique. In the remainder

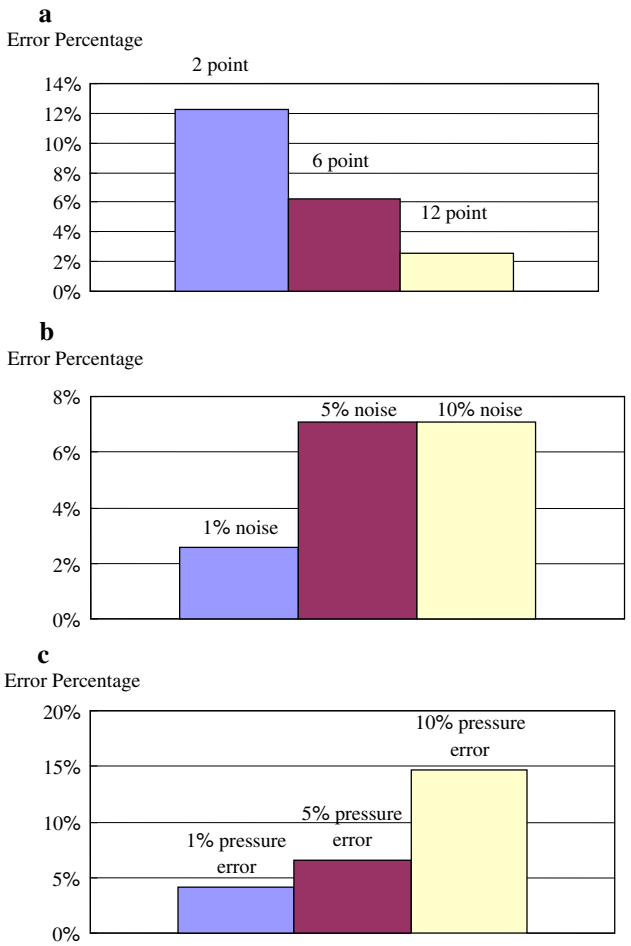

Fig. 4 Sensitively analysis of the random exhaustive search (RES) algorithm to the measurement noise and error. Overall error in parameter estimation defined as the average error among all the parameters excluding the error associated with the lipid pool. **a** Comparison of 2-point, 6-point and 12-point methods subject to 1% white Gaussian noise of strain. **b** Trend of error percentage increases up to 7% when strain noise increases from 1% to 5% and 10%, while using a 12-point method. **c** Effect of the pressure error on the overall error in the parameter estimation, while using a 12-point method

of this paper, the 12 point algorithm is used for parameter estimation. The parameter estimation error increased as the underlying (imposed) noise was elevated from 1% to 5% and 10% (see Fig. 4b). At a 10% noise, the maximum error level was less than 7% which is reasonably small (Williamson et al. 2003). This suggests that the algorithm is robust and shows a reasonably low sensitivity to the noise in the strain data. Although no comparable algorithm exists for nonlinear models, the present algorithm is in general less sensitive to strain noise when compared with the calculus-based ones for linear elastic models (Doyley et al. 2000; Kallel and Bertrand 1996; Khalil et al. 2005; Oberai et al. 2004). We next tested the sensitivity of the algorithm to the error in pressure measurement (see Fig. 4c). A 5% or 10% uncertainty in the pressure data yielded overall error levels up to 5% or 15%. That is, the algorithm is nonlinearly sensitive to pressure error and care must be exercised to keep the pressure uncertainty to a minimum.

To test the performance of the present scheme in estimating the mechanical properties of plaques in 3D, a preliminary study was conducted using our idealized 3D geometry. The error average between the real and estimated mechanical properties for intra-plaque regions, excluding the lipid region, was 3.6% (Table 3). The present results suggest the viability of our algorithm in 3D models. Further investigation is needed to verify the feasibility of the algorithm in realistic 3D applications in the presence of noise.

Genetic Algorithm

Our GA-based parameter estimation algorithm for linear mechanical models (Khalil et al. 2006) was extended to analyze nonlinear models, incorporating a new mutation operator. Hence, like RES at least after infinite number of evaluations, the scheme should accurately find the global minimum, but with a smarter search and a lower computational cost.

To test the performance of the GA method for nonlinear parameter estimation, we first limited our search solely to D_1, by assuming a known D_2 value. This was carried out with initial populations of either 16 or 40 individuals (see

Table 3 Estimated properties of 3D noise-free model using 2-point RES

Mooney-Rivlin parameters	2-point estimated results	
	D_1 [Pa] (error)	D_2 (error)
Arterial wall	2801.0 (5.9%)	8.4 (1.2%)
Fibrous plaque	5084.9 (0.4%)	12.1 (6.9%)
Lipid	57.0 (14.0%)	0.46 (8.0%)

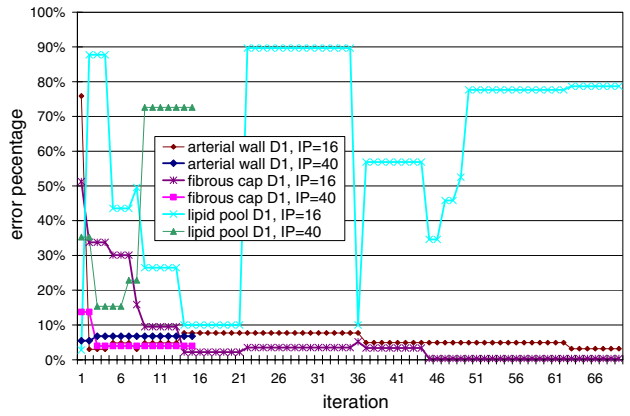

Fig. 5 GA convergence of the three parameters of the nonlinear lumped model with prescribed D_2 value at two different populations size

Fig. 5). As in the linear elastic case, as well as the nonlinear problem solved by RES, GA-based results for lipid parameters are subject to larger errors. The errors in estimation of parameters other than in the lipid pool were approximately 5%, after nearly 200 simulation calls to the FEM solver; which is comparable with the linear-elastic results (we used about 250–500 calls for linear case; Khalil et al. 2006).

To achieve a certain accuracy level with minimal computational cost, an optimal population number exists; as too small or too large population sizes are both practically inefficient (see Fig. 6). However, the difference between initial population of sizes 40 and 16 is negligible. By using the initial population size (IP) of 40, the initial stationary solution is closer to the true value than that using IP = 16; but after about 200 FEM simulation runs, both have achieved reasonable accuracy (~5% error). It must be remarked that the introduction of mutation operator may yield abrupt changes in solution, which will, of course, eventually yield better final accuracy. The results show that GA can be used for efficient estimation of one parameter of a nonlinear model by using one loading point. Next we focus our attention toward estimation of two parameters (6 unknowns) using the multipoint technique and fixing initial population to 40 individuals. Note that the initial search field covers 10 folds (see Table 1), which is up to 5 times larger compared to the RES search range. In fact, RES did not generate satisfying results with such a large search field.

The utility of multipoint technique for one and two parameters estimations is demonstrated in Fig. 7. The 1-,2- or 4-point techniques produced similar results for the one-unknown case. For the two-unknown case, at least 2 loading points are required, and extra points can reduce the estimation error. With the 4-point technique, the error reaches less than 10% after 28 iterations (Fig. 7). By using the 1-point technique, the algorithm failed to converge on the true values. The 2-point method improves the accuracy of nonlinear parameter estimation. Yet, to deal with noise which is inevitable (even in the current study where simulated strain maps are employed), at least 4 loading points were needed to substantially improve the performance of the algorithm. It is worth noting that the number of frames or loading points used in the algorithm does not necessarily increase the computational cost of the overall parameter estimation procedures, given that nonlinear FEM computations require incremental application of load (here we needed 24 load steps).

As mentioned previously, GA can perform the estimation within a much wider range of possible values as compared to RES. The efficiency of these two methods for the same search field and the same number of loading points (namely 4) were next compared. Both methods were eventually able to capture the true values but at different

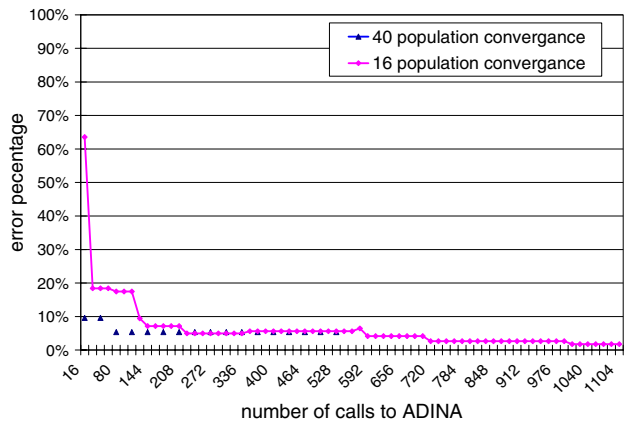

Fig. 6 GA convergence of the overall error index of the three parameters nonlinear model versus the total call to ADINA for different population sizes

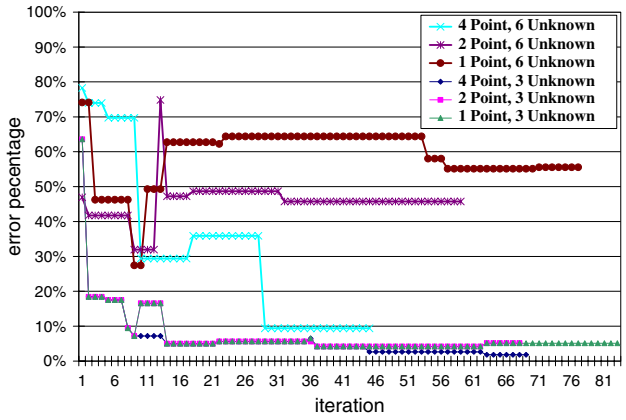

Fig. 7 GA convergence with different degrees of multipoint and different number of unknowns. Overall error in parameter estimation defined as the average error among all the parameters excluding the error associated with the lipid pool

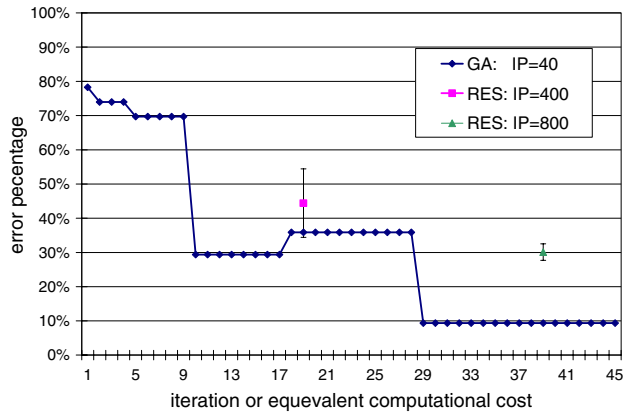

Fig. 8 Computational efficiency of RES versus GA, both based on using 4 points. Note that standard deviation for RES is based on 8 runs. Overall error in parameter estimation defined as the average error among all the parameters excluding the error associated with the lipid pool

rates. Higher efficiency and lower error bounds were observed with GA (Fig. 8). However, it must be noted that due to the randomness in generating the initial population, the results of RES may vary. Hence, standard deviations are calculated for the RES results, each based on 8 independent runs.

As shown previously, with the RES method, extra loading points can be employed to reduce the effect of the image noise. For example, with a low image noise of 1% increasing the number of multiple points from 2 to 12 lowered the estimation parameter by 2-fold. Higher levels of noise were tested, showing that eventually estimation fails for a 5% noise; even if we use 12 loading points. This indicates that image noise will play the major limiting role in the application of the GA multipoint technique.

It must be noted that the RES method is successful for 10% image noise and has also a lower error in 1% noise (see Figs. 4b, 9). At the first glance this may sound

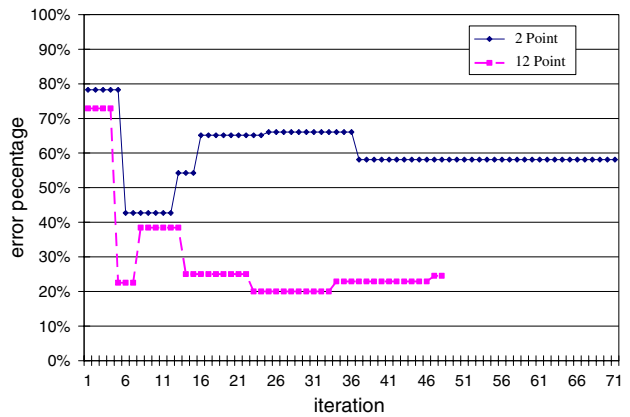

Fig. 9 Comparison of GA convergence for a noisy image: a 2-point method with a 12-point one

surprising but in fact it is only an artifact caused by unequal search regions for RES and GA. Comparing the search domain for RES and GA (Table 1), one notices that GA is covering a domain about 5 times larger in each direction. Consequently, using equal search domains for RES and GA can yield similar or superior performance in GA in dealing with the noise issue. This is of course expected as the GA algorithm is a smarter method as compared to RES. Interestingly, while GA is producing reasonable solutions for its large domain, RES was not at all applicable (with current population size) to tackle GA large domain.

Following the same line of argument we can realize that since RES is applicable to the 3D model, GA would be naturally applicable as well. Furthermore, it must be noted that 3D models, which can be viewed as a collection of 2D sections, have in general a larger number of elements, i.e. more multi-point input, and hence we expect 3D model to be less sensitive to noise.

We have not compared RES and GA schemes with respect to pressure uncertainties. It must be remarked however that pressure error is mostly a fixed scaling error uniformly applied to all elements, regardless of the chosen scheme. On the other hand image noise has a totally different nature and it is a random error, affecting different elements nonuniformly and randomly.

Discussion

To mimic the strain-stiffening behavior of vascular tissues, nonlinear constitutive models must be used. The GA method, described earlier (Khalil et al. 2006) as a robust and efficient means for parameter estimation, was extended here to incorporate material models with nonlinear constitutive relations. Unlike calculus-based techniques for parameter estimation, GA is a straight-forward and efficient scheme, especially when applied to a model system that features a reasonable number of lumped parameters. Several numerical experiments were conducted to evaluate the accuracy and noise sensitivity of the present GA-based approach.

It is worthwhile to compare our GA scheme for linear applications (Khalil et al. 2006) with the present GA-based nonlinear estimation approach. Here we have incorporated mutation and multipoint techniques with more realistic geometries. In our linear models (Khalil et al. 2006), we based our analysis on an initial population of 100 and up to 4 unknowns, corresponding to 4 lumped regions. Here we use an initial population of 40 with mutation and up to 6 unknowns. As a result, our previous calculations converged with at most 8 iterations while here at least 30 iterations are required. This is because enough randomness cannot be guaranteed just by enlarging the initial population and one

has to rely on mutation. Also in our linear work we modified survival probability and weights of different regions in fitness function to improve higher error in softer regions (lipid). This was not implemented here but it is similarly applicable and can be used to reduce error in soft tissue estimation. Finally, while it is not trivial to compare two approaches with respect to the noise, given the models' different natures, the noise error seems to be lower here due mainly to multipoint technique (Fig. 4).

Our 2D models, incorporating OCT-based subject-specific coronary slices (Chau et al. 2004), involved plain strain element, which is only valid if the vessel is either constrained longitudinally or if the longitudinal dimension is sufficiently large and the longitudinal strains are negligible. Since the elastography data was generated with the same 2D FEM analysis, this does not influence the parameter estimation results. This may not be the case in vivo, as some segments of coronary vessels can undergo curvature changes during the cardiac cycle. Axial variations in plaque geometry might also significantly alter stress and strain fields, possibly affecting the accuracy of FEM analysis and the overall parameter estimation algorithm. Due to this consideration, 3D FEM analysis was preliminarily investigated and the robustness of the algorithm and its applicability to more complex and realistic FEM models was demonstrated. However, the out-of-plane strain is extremely difficult to obtain from 3D elastography, due to the challenges in correlating the pixels between adjacent slices during pullback. This could become a serious obstacle that limits the accuracy of 3D estimation and that is why we have only used plane strains for the fitness function.

Another limitation of the present study is that the residual strain was not considered. Unlike linear elastic models, the presence of residual strain plays a major role in nonlinear ones. In the current study, elastography data obtained from the FEM model were used and hence neglecting the residual strains does not affect the parameter estimation algorithm. However, due to the lack of an accurate model to quantify the residual strains in an artery, it is difficult to assess the residual strain noninvasively. A recent study found that the cyclic strain distribution remains relatively unchanged by the inclusion of residual stress (Kaazempur-Mofrad et al. 2003). Nonetheless, the influence of residual strain on the nonlinear mechanical property estimation remains to be rigorously addressed.

In the current study, we performed quasi-static FEM analysis where the applied pressure load was incrementally raised. This is a valid assumption for ex vivo elastography, where the pressure load is applied slowly. However, for the in vivo case due to the blood pressure oscillation, the dynamic effects of the vessel wall and/or blood and tissue surrounding it might not be negligible. Viscoelastic models might also be needed for dynamic analysis, especially for the lipid pool component of the plaques (Loree et al. 1994). Such nonlinear dynamic analyses are much easier to implement in GA with lumped parameter models than calculus-based methods.

The multipoint scheme was introduced in this study to determine the nonlinear material model, and was used as an effective means for decreasing the sensitivity to noise. This feature is not only useful for nonlinear material model; but also can be applied for the estimation of linear elastic models, much like increasing regression points for a linear fit. GA was proven to be a viable and relatively efficient method, but the image noise and pressure uncertainty strongly affects the accuracy of the estimation.

Although the multipoint scheme may be helpful to resolve the noise issue, the real cases might be far more complicated than simple models we tested here. Hence, noise is still the biggest obstacle in developing such an estimation method. Work is in progress in our laboratory to develop new techniques for robust elastography, exploiting kinematics and mechanics of incompressible tissues directly into image registration step to compute strains (Chan et al. 2004; Karimi et al. 2006).

Unfortunately, the level of noise in OCT elastography is not yet well characterized. The noise can vary based on laser quality, system calibration, tissue types, loading rates, rigid body motion and even strain level. More importantly, the noise will vary inversely with strain resolution and the imposed regularity constraints during image registration (Chan et al. 2004). Regularity constraints impose additional criteria like incompressibility, strain uniformity and lower levels of strain gradients to ensure that registration process generates a physically meaningful displacement field (Chan et al. 2004). If we use a larger window size for image registration or median filtering, then the noise will be filtered out as well as the fine details of displacement. Penalizing the incompressible strain and strain gradients leads to a lower noise but is also accompanied by suppressing some high spatial frequency components of the desired signal. Unfortunately, it is not trivial to define the noise for a real setup because there is no other alternative method to measure the strain, unless we test a uniform sample, then the problem is that our priori knowledge might lead to increasing weights of the regularity constraints which enforce uniformity (Chan et al. 2004). Hence, the regularity settings are often prescribed and then the noise effect on different samples is typically examined (Chan et al. 2004; Khalil et al. 2005; Schmitt 1998). As well demonstrated in our earlier publication, the noise can vary from 100% error to 1% error, depending on the registration techniques and other settings (Chan et al. 2004). Fortunately, reducing our strain resolution can lead to low levels of strain noise, namely even below 5%. Therefore,

while the typical resolution of OCT is about 15 μm, the strain will be evaluated at a resolution about 150 μm or larger. This might not work for conventional elastography where elastic properties are evaluated at a fine mesh, but here we are using a lumped model with a relatively large length scale and therefore expecting little complication.

Further, it must be noted that pixilated images yield spatially nonuniform errors in image registration, corresponding to the nonhomogeneous magnitude of displacements and displacement gradients during image registration. However, it seems that if we use different frames of varying displacement magnitude, those errors will be cancelled out and the overall result of registration can be more accurate and more reliable. Indeed this is another advantage of multi-point technique.

It should be noted that incorporating multiple loading points for multiple parameter estimation is a necessary condition to assure solution uniqueness according to degrees of freedom in elasticity curve. However, this is not a sufficient condition for the inverse problem with a fine mesh. Indeed, even for incompressible homogenous linear elastic materials (one unknown), there is no unique solution associated with one frame for practical loading cases (Barbone and Bamber 2002). In that case, it is proved that for a 2D problem, using four independent loading conditions and measuring one component of displacement, a solution with only one arbitrary unknown constant can be constructed (Barbone and Gokhale 2004). However, in practical cases it would be difficult to apply four independent loading conditions to a linear material. On the other hand, our multipoint technique, applied to nonlinear material, can generate better results not only due to robustness to noise, but also due to the higher chance for construction of the unique solution of the inverse problem.

Realistically, tissue mechanical properties are continuous and inhomogeneous in space. Lumping parameters is a strong assumption and can lead to artificial stress concentrations that undermine the viability of this method in assessing the plaque vulnerability. However, the overall algorithm can still serve as a pseudo-regularization technique, providing a robust and accurately preconditioned initial guess as the low-resolution component of a multi-resolution scheme. In addition, when provided with the in vivo elastography data via OCT or high resolution MRI, this algorithm can estimate the lumped patient-specific mechanical properties by a minimally invasive or noninvasive method and utilize those for medical correlations (Schaar et al. 2004). For instance, ex vivo studies have observed that lipid's mechanical properties are influenced by its components (Loree et al. 1994) and therefore are very patient/case specific. Monitoring the change of such parameters in vivo allows for longitudinal studies that can potentially increase our understanding of the physiological change of the tissue during the progression of atherosclerosis. By differentiating the mechanical characteristics of the vascular tissues with high or low risk of plaque rupture, it is possible to set up a diagnostic tool for assessment of plaque vulnerability that partly relies on the distribution of the stress/strain as well as plaque geometry and composition (Fig. 1).

Acknowledgements This study was funded by the National Institutes of Health (Grant 5-R01-HL70039). Fruitful discussions with Dr. Roger D. Kamm are gratefully acknowledged.

References

Baldewsing RA, Schaar JA, de Korte CL, Mastik F, Serruys PW, van der Steen AF. Intravascular ultrasound elastography: a clinician's tool for assessing vulnerability and material composition of plaques. Stud Health Technol Inform. 2005;113:75–96.

Barbone PE, Bamber JC. Quantitative elasticity imaging: what can and cannot be inferred from strain images. Phys Med Biol. 2002;47:2147–2164.

Barbone PE, Gokhale NH. Elastic modulus imaging: on the uniqueness and nonuniqueness of the elastography inverse problem in two dimensions. Inverse Probl. 2004;20:283–296.

Bathe K-J. Finite element procedures. Upper Saddle River, New Jersey: Prentice Hall; 1996.

Chan RC, Chau AH, Karl WC, Nadkarni S, Khalil AS, Iftimia N, et al. OCT-based arterial elastography: robust estimation exploiting tissue biomechanics. Opt Express. 2004;12:4558–4572.

Chau AH, Chan RC, Shishkov M, MacNeill B, Iftimiia N, Tearney GJ, et al. Mechanical analysis of atherosclerotic plaques based on optical coherence tomography. Ann Biomed Eng. 2004;32:1494–1503.

Doyley MM, Meaney PM, Bamber JC. Evaluation of an iterative reconstruction method for quantitative elastography. Phys Med Biol. 2000;45:1521–1540.

Draney MT, Herfkens RJ, Hughes TJ, Pelc NJ, Wedding KL, Zarins CK, et al. Quantification of vessel wall cyclic strain using cine phase contrast magnetic resonance imaging. Ann Biomed Eng. 2002;30:1033–1045.

Duck FA. Physical properties of tissues—a comprehensive reference book. Sheffield, United Kingdom: Academic Press; 1990.

Fercher AF, Drexler W, Hitzenberger CK, Lasser T. Optical coherence tomography—principles and applications. Rep Prog Phys. 2003;66:239–303.

Haupt RL, Haupt SE. Practical genetic algorithms. New York, NY: Wiley; 2004.

Huang H, Virmani R, Younis H, Burke AP, Kamm RD, Lee RT. The impact of calcification on the biomechanical stability of atherosclerotic plaques. Circulation. 2001;103:1051–1056.

Kaazempur-Mofrad MR, Younis HF, Patel S, Isasi A, Chung C, Chan RC, et al. Cyclic strain in human carotid bifurcation and its potential correlation to atherogenesis: idealized and anatomically realistic models. J Eng Math. 2003;47:299–314.

Kallel F, Bertrand M. Tissue elasticity reconstruction using linear perturbation method. IEEE Trans Med Imaging. 1996;15:299–313.

Karimi R, Chan R, Houser S, Bouma BE, Kaazempur Mofrad MR. A novel framework for elastography and modulus estimation: integration of tissue mechanics with imaging. 2006 IEEE

International Symposium on Biomedical Imaging: From Macro to Nano, Arlington, Virginia, USA. IEEE; 2006. p. 602–605.

Kawase Y, Hoshino K, Yoneyama R, McGregor J, Hajjar RJ, Jang I-K, et al. In vivo volumetric analysis of coronary stent using optical coherence tomography with a novel balloon occlusion-flushing catheter: a comparison with intravascular ultrasound. Ultrasound Med Biol. 2005;31:1343–1349.

Khalil AS, Chan RC, Chau AH, Bouma BE, Mofrad MR. Tissue elasticity estimation with optical coherence elastography: toward mechanical characterization of in vivo soft tissue. Ann Biomed Eng. 2005;33:1631–1639.

Khalil AS, Bouma BE, Kaazempur Mofrad MR. A combined FEM/genetic algorithm for vascular soft tissue elasticity estimation. Cardiovasc Eng. 2006;6:93–102.

Lee RT, Loree HM, Cheng GC, Lieberman EH, Jaramillo N, Schoen FJ. Computational structural analysis based on intravascular ultrasound imaging before in vitro angioplasty: prediction of plaque fracture locations. J Am Coll Cardiol. 1993;21:777–782.

Lee RT, Schoen FJ, Loree HM, Lark MW, Libby P. Circumferential stress and matrix metalloproteinase 1 in human coronary atherosclerosis. Implications for plaque rupture. Arterioscler Thromb Vasc Biol. 1996;16:1070–1073.

Loree HM, Kamm RD, Stringfellow RG, Lee RT. Effects of fibrous cap thickness on peak circumferential stress in model atherosclerotic vessels. Circ Res. 1992;71:850–858.

Loree HM, Tobias BJ, Gibson LJ, Kamm RD, Small DM, Lee RT. Mechanical-properties of model atherosclerotic lesion lipid pools. Arterioscler Thromb. 1994;14:230–234.

Nighoghossian N, Derex L, Douek P. The vulnerable carotid artery plaque: current imaging methods and new perspectives. Stroke. 2005;36:2764–2772.

Oberai AA, Gokhale NH, Doyley MM, Bamber JC. Evaluation of the adjoint equation based algorithm for elasticity imaging. Phys Med Biol. 2004;49:2955–2974.

Ophir J, Cespedes I, Ponnekanti H, Yazdi Y, Li X. Elastography: a quantitative method for imaging the elasticity of biological tissues. Ultrason Imaging. 1991;13:111–134.

Ophir J, Kallel F, Varghese T, Bertrand M, Cespedes I, Ponnekanti H. Elastography: a systems approach. Int J Imaging Syst Technol. 1997;8:89–103.

Richardson PD, Davies MJ, Born GV. Influence of plaque configuration and stress distribution on fissuring of coronary atherosclerotic plaques. Lancet. 1989;2:941–944.

Rivlin RS. Large elastic deformations of isotropic materials IV. Further developments of the general theory. Philos Trans R Soc Lond. 1948;A 241:379–397.

Rogowska J, Patel NA, Fujimoto JG, Brezinski ME. Optical coherence tomographic elastography technique for measuring deformation and strain of atherosclerotic tissues. Heart. 2004;90:556–562.

Schaar JA, de Korte CL, Mastik F, Baldewsing R, Regar E, de Feyter P, et al. Intravascular palpography for high-risk vulnerable plaque assessment. Herz. 2003;28:488–495.

Schaar JA, Regar E, Mastik F, McFadden EP, Saia F, Disco C, et al. Incidence of high-strain patterns in human coronary arteries: assessment with three-dimensional intravascular palpography and correlation with clinical presentation. Circulation. 2004;109:2716–2719.

Schmitt JM. OCT elastography: imaging microscopic deformation and strain of tissue. Opt Express. 1998;3:199–211.

Sinkus R, Tanter M, Catheline S, Lorenzen J, Kuhl C, Sondermann E, et al. Imaging anisotropic and viscous properties of breast tissue by magnetic resonance-elastography. Magn Reson Med. 2005;53:372–387.

Tearney GJ, Jang IK, Bouma BE. Optical coherence tomography for imaging the vulnerable plaque. J Biomed Opt. 2006;11:021002.

Thom T, Haase N, Rosamond W, Howard VJ, Rumsfeld J, Manolio T, et al. Heart disease and stroke statistics-2006 update: a report from the American Heart Association Statistics Committee and Stroke Statistics Subcommittee. Circulation. 2006;113:e85–e151.

Wang RK, Kirkpatrick S, Hinds M. Phase-sensitive optical coherence elastography for mapping tissue microstrains in real time. Appl Phys Lett. 2007;90:164105. (164103 Pages).

Williamson SD, Lam Y, Younis HF, Huang H, Patel S, Kaazempur-Mofrad MR, et al. On the sensitivity of wall stresses in diseased arteries to variable material properties. J Biomech Eng-Trans ASME. 2003;125:147–155.

Yabushita H, Bouma BE, Houser SL, Aretz HT, Jang IK, Schlendorf KH, et al. Characterization of human atherosclerosis by optical coherence tomography. Circulation. 2002;106:1640–1645.

Yun SH, Tearney GJ, de Boer JF, Iftimia N, Bouma BE. High-speed optical frequency-domain imaging. Opt Express. 2003;11:2953–2963.

Yun SH, Tearney GJ, Vakoc BJ, Shishkov M, Oh WY, Desjardins AE, et al. Comprehensive volumetric optical microscopy in vivo. Nat Med. 2006;12:1429–1433.